



Cite this: DOI: 10.1039/d6bm00261g

# Hybrid cell membrane-conjugated photosensitive hydrogels as a tumor vaccine for promoting cancer immunotherapy

Chaoying Wang,<sup>a</sup> Tao Wang,<sup>†b</sup> Wenxin Zhou,<sup>†a</sup> Yanxu Li,<sup>a</sup> Weiben Ji,<sup>a</sup> Shengyi Wu,<sup>a</sup> Yutao Feng,<sup>a</sup> Lai Chang,<sup>a</sup> Quan Zhang<sup>\*b</sup> and Wei Wu<sup>\*a</sup>

Preventive tumor vaccines exhibit substantial potential in averting tumorigenesis; nevertheless, their clinical efficacy remains constrained by challenges in eliciting potent and long-lasting immune activation, which ultimately leads to subpar overall therapeutic performance. In this study, we designed a biofilm-based hydrogel as a highly efficient single-dose prophylactic tumor vaccine. A hybrid biofilm (TMBM), which combines bacterial membrane (BM) and tumor cell membrane (TM), was modified with methacrylated hyaluronic acid–gelatin methacrylate (HAMA–GelMA) to form a gel formulation (HG–TMBM hydrogel). This hydrogel can encapsulate ginsenoside Rg3 (Rg3) within its micropores and rapidly gelate *in situ* following subcutaneous injection. Upon single administration of the HG–TMBM hydrogel/Rg3 vaccine, both TMBM and Rg3 are sustainably released owing to the degradable nature of the HAMA–GelMA matrix. TMBM actively targets dendritic cells (DCs) and efficiently induces their maturation. Concurrently, Rg3 modulates the immune microenvironment and enhances antigen presentation efficiency, providing robust support for subsequent antigen cross-presentation. Ultimately, the vaccine successfully elicits potent and long-lasting T lymphocyte-mediated immune responses and exhibits significant preventive efficacy against colon tumors. The present work constructs a sustained-action system for tumor prophylaxis, offering an innovative approach for the creative development of single-administration preventive tumor vaccines.

Received 23rd February 2026,  
Accepted 13th April 2026

DOI: 10.1039/d6bm00261g

rsc.li/biomaterials-science

## 1. Introduction

The core function of cancer vaccines is to elicit immune responses against tumor-associated antigens, which are characteristic protein structures of tumor cells.<sup>1–3</sup> Tumor-specific antigens are expressed exclusively on tumor cell membranes and can induce the activation of T lymphocytes and the differentiation of CD8<sup>+</sup> cytotoxic T lymphocytes (CTLs), exerting targeted anti-tumor effects.<sup>4</sup> Adjuvants are key components of vaccines. Ideal adjuvants can regulate antigen retention, concentration, and presentation efficiency of antigen-presenting cells (APCs) to activate the first signal of T cells, and enhance the co-stimulation and cytokine secretion capacity of APCs.<sup>5,6</sup> As the most potent APCs, dendritic cells can take up and process antigens, present them *via* MHC class I and II

molecules, and activate T lymphocyte subsets.<sup>7,8</sup> Compared with radiotherapy and chemotherapy, they cause less damage to normal tissues and can reduce tumorigenesis risk at the source. However, traditional cancer vaccines suffer from weak immune activation, poor durability, easy degradation of active components, and the requirement for multiple inoculations, leading to unsatisfactory immune responses in some patients due to immune tolerance.<sup>9</sup> Therefore, the development of novel cancer vaccines with high immunogenicity is of great significance for tumor prevention and treatment.

In recent years, the fields of biomedical materials and cancer therapy have witnessed numerous advances in biomimetic delivery systems, composite hydrogels, and immunotherapy. Relevant studies have systematically reviewed polymer hydrogel composites and chemotherapeutic drug delivery carriers.<sup>10,11</sup> Meanwhile, nanoplatforms and injectable hydrogels have been employed to achieve tumor-targeted therapy, immune activation, and remodeling of the immune microenvironment.<sup>12,13</sup> In the area of biomimetic immunotherapy, the applications of cell membrane biomimetic systems and bacterial outer membrane vesicles in cancer vaccines have also been extensively explored, providing important

<sup>a</sup>General Surgery, The Affiliated Hospital of Yangzhou University, Yangzhou University, 368 Hanjiang Middle Road, Hanjiang District, Yangzhou City, Jiangsu Province, 225000, China. E-mail: 306834397@qq.com

<sup>b</sup>College of Veterinary Medicine, Yangzhou University, No. 48 Wenhui East Road, Yangzhou, Jiangsu Province, 225000, China. E-mail: zquan@yzu.edu.cn

<sup>†</sup>These authors contributed equally to this work.



theoretical and experimental support for the development of hydrogel vaccines, biomimetic delivery systems, and tumor chemoimmunotherapy.<sup>14,15</sup>

Biofilms have shown considerable application potential in tumor therapy by virtue of their unique biological activities inherited from their original cells.<sup>16</sup> Tumor cell membranes (TMs) are rich in tumor-specific antigens and serve as an ideal antigen source for vaccines. However, their intrinsic immunogenicity is relatively weak, making it difficult to effectively activate immune responses *in vivo*.<sup>17</sup> Bacterial membranes (BMs) contain active components such as lipopolysaccharides and lipoproteins, which can activate the TLR4/TLR2 signaling pathway and efficiently induce the maturation of dendritic cells, making them excellent immune adjuvants.<sup>18</sup> Hybrid cell membranes integrate the antigen diversity and immunomodulatory functions of different cell membranes. By fusing tumor cell membranes with bacterial or immune cell membranes, they can simultaneously deliver dual signals of antigens and adjuvants to antigen-presenting cells, overcoming the limitations of traditional subunit vaccines.<sup>19</sup> As the main active component of red ginseng, ginsenoside Rg3 (Rg3) exhibits remarkable immunomodulatory effects. It can enhance antigen presentation efficiency, promote CTL activation, and simultaneously inhibit tumor cell proliferation, invasion, and induce apoptosis and autophagy.<sup>20,21</sup> Hydrogel carriers enable spatiotemporally controlled delivery of therapeutic agents. Among them, injectable HAMA–GelMA interpenetrating network hydrogels feature stable encapsulation, rapid gelation, and favorable biocompatibility, allowing long-term sustained drug release.<sup>22–24</sup>

Based on the above strategy, this study constructed an injectable hybrid biofilm hydrogel as a prophylactic colon cancer vaccine. The hybrid biofilm (TMBM) prepared by fusing tumor cell membranes (TMs) and bacterial membranes (BMs) can provide both tumor antigen and immune adjuvant functions. TMBM, ginsenoside Rg3 and HAMA–GelMA were combined to form the HG-TMBMR hydrogel, which can rapidly gel *in situ* under blue light irradiation, achieving stable encapsulation of TMBM and Rg3. During the gradual degradation of the hydrogel matrix, TMBM and Rg3 were released in a long-term sustained manner. TMBM can target dendritic cells and promote their maturation, while Rg3 improves the immune microenvironment, enhances antigen presentation efficiency, and strengthens CTL-mediated anti-tumor immunity.<sup>25</sup> A single inoculation of HG-TMBMR induces potent and long-lasting T-cell immunity and effectively prevents colon cancer, providing a new strategy for the development and clinical translation of single-dose prophylactic tumor vaccines (Fig. 1).

## 2. Methods

### 2.1 Preparation of the tumor cell membrane (TM)

CT26 monolayers were rinsed once with PBS buffer. Adherent cells were detached by mechanical scraping or incubation in an EDTA-supplemented, trypsin-free dissociation buffer, fol-

lowed by gentle aspiration to release the cells. The suspension was centrifuged, the supernatant was discarded, and the resulting cellular sediment was retained. Membrane fragments were isolated using a Membrane Protein and Cytoplasmic Protein Extraction Kit (Beyotime Biotechnology). The pelleted material was re-dispersed in PBS, passed 11 times through a polycarbonate filter bearing 400 nm pores with an Avanti mini-extruder, and subsequently preserved at  $-20\text{ }^{\circ}\text{C}$ .

### 2.2 Preparation of the bacterial membrane (BM)

A 250 mL volume of MRS broth was seeded with *Lactobacillus reuteri* (*L. reuteri*) and maintained at  $37\text{ }^{\circ}\text{C}$  under continuous orbital shaking. After the culture achieved an absorbance of 1.2 at 600 nm, the cells were pelleted *via* centrifugation at 5000 rpm for 10 minutes. Following washing, the bacteria were resuspended in PBS, and the bacterial suspension was disrupted using an ultrasonic cell disruptor (pulse: 5 s on and 10 s off, for 90 min at  $0\text{ }^{\circ}\text{C}$ ). After sonication, the suspension was centrifuged at  $14\ 000g$  for 20 min at  $4\text{ }^{\circ}\text{C}$ . The collected precipitate was resuspended in PBS and extruded 11 times through a polycarbonate porous membrane (400 nm pore size) using an Avanti mini-extruder, and then stored at  $-20\text{ }^{\circ}\text{C}$ .

### 2.3 Preparation and characterization of TMBM

The tumor cell membrane (TM) and bacterial membrane (BM) were dispersed in ultrapure water at a mass ratio of 5 : 1. Following sonication of the preparation for 30 minutes at  $20\text{ }^{\circ}\text{C}$  using a 300 W ultrasonic apparatus (model KQ-300DE), the material underwent 11 extrusion cycles through a polycarbonate filter with 400 nm pores *via* an Avanti mini-extruder. Centrifugation at 12 000 rpm and  $4\text{ }^{\circ}\text{C}$  for 30 min was subsequently performed to harvest the hybrid biofilm, hereafter referred to as TMBM. To verify the hybrid fusion of the two biofilms, TM and BM were labeled with 1,1'-dioctadecyl-3,3,3',3'-tetramethylindodicarbocyanine perchlorate (DiD) and 3,3'-dioctadecyloxycarbocyanine perchlorate (DiO), respectively. TMBM was fabricated following the aforementioned protocol, and confocal microscopy was utilized to examine the colocalization of the dual fluorescent signals.

For TM, BM, and TMBM samples, membrane proteins were thoroughly extracted using a Membrane Protein and Cytoplasmic Protein Extraction Kit (Beyotime Biotechnology). Protein levels across distinct preparations were quantified using a bicinchoninic acid (BCA)-based assay. Comparative profiling of the polypeptide composition in the TM, BM, and TMBM was carried out *via* SDS-PAGE. Each specimen, normalized for the total protein content, was supplemented with a concentrated sample buffer containing dithiothreitol and a tracking dye, incubated at ambient temperature for 30 minutes to ensure denaturation, and subsequently electrophoresed on 12% polyacrylamide resolving gels. Following electrophoresis, the gel was stained with Coomassie Brilliant Blue for 3 h and destained overnight in a diluted destaining solution, and then imaged using a Bio-Rad Gel Doc XR + gel imaging system.



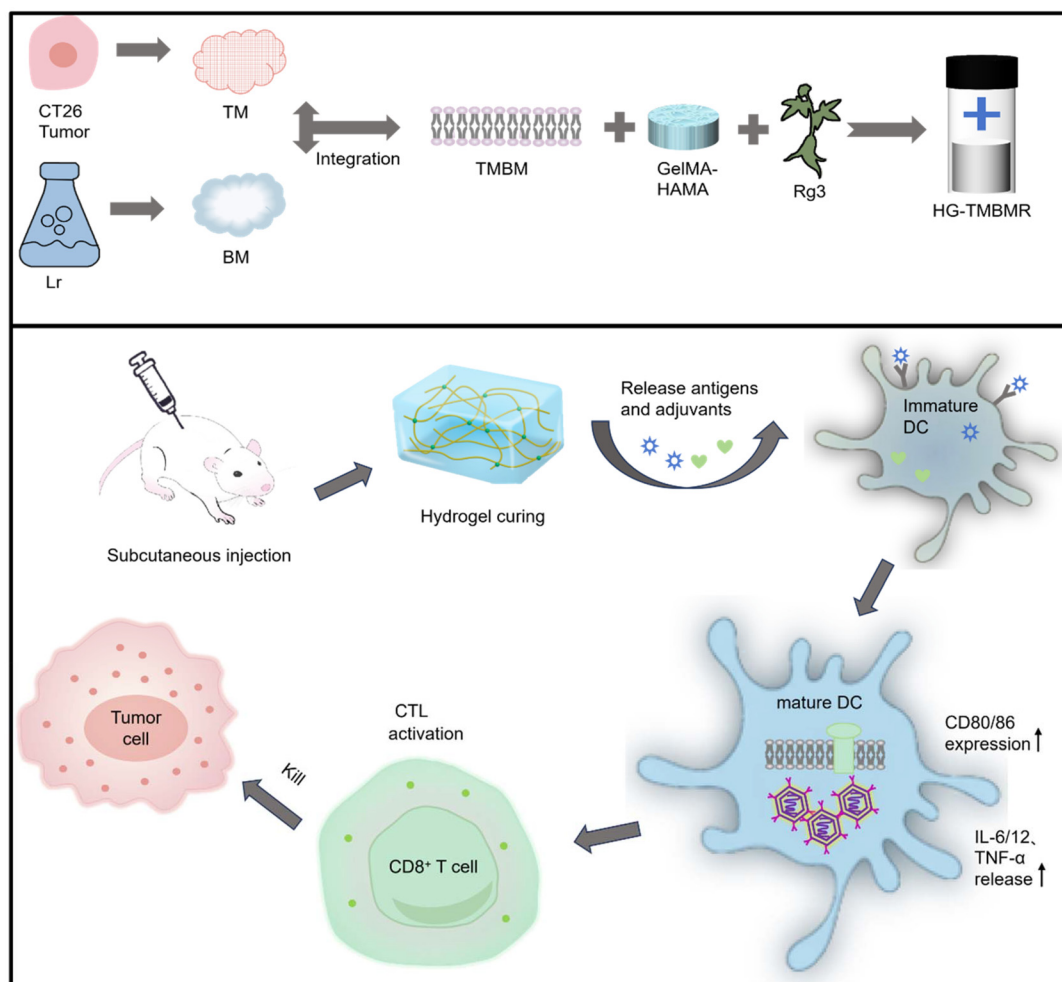


**Fig. 1** Schematic representation of the biofilm-derived HG-TMBMR injectable hydrogel vaccine, which facilitates dendritic cell (DC) maturation, enhances antigen cross-presentation, and stimulates T-cell activation.

#### 2.4 Preparation and characterization of the HG-TMBMR hydrogel

Methacrylated hyaluronic acid (HAMA) and gelatin methacrylate (GelMA) were purchased from Suzhou Xianjue New Material Technology Co., Ltd. Hydrogel precursor solutions were formulated according to the supplied protocol. To verify whether the system can achieve rapid gelation, the vortexed solution was mixed with TMBM and Rg3, and exposed to 405 nm blue light for 60 seconds. Approximately 100  $\mu\text{L}$  of HG-TMBMR hydrogel solution containing a small amount of phenol red was drawn using a 1 mL syringe and injected at a constant rate into a phosphate-buffered saline (PBS) solution to evaluate the injectability through a 27-gauge (27 G) 0.45 mm needle. Following complete gel solidification, the specimen was stored at  $-80\text{ }^\circ\text{C}$  for 12 hours and subsequently subjected to lyophilization. The sample was sectioned and observed by scanning electron microscopy (SEM).

#### 2.5 *In vitro* release of encapsulated components from hydrogels

Bovine serum albumin (BSA) was solubilized to a final concentration of  $1.5\text{ mg mL}^{-1}$ . A 0.1 mL aliquot of this protein solu-

tion was introduced into 1 mL of the gel precursor formulation. Following photo-crosslinking triggered by 405 nm blue light exposure, the resulting hydrogel was placed in phosphate-buffered saline (PBS, pH 6.8) and maintained at  $37\text{ }^\circ\text{C}$  under orbital agitation. At designated intervals, aliquots were withdrawn, and the corresponding protein content was determined using a Bradford-based assay.

#### 2.6 *In vivo* subcutaneous degradation behavior

All animal procedures were performed in accordance with the Guidelines for Care and Use of Laboratory Animals of Yangzhou University and approved by the Animal Ethics Committee of Yangzhou University (no. 202508003). The HG-TMBMR hydrogel (100  $\mu\text{L}$ ) was subcutaneously injected into BALB/c mice. Mice were euthanized at predetermined time points to observe the *in vivo* degradation behavior of the hydrogel.

#### 2.7 *In vivo* retention effect

Following covalent conjugation with the lipophilic NIR fluorophore DiR (1,1'-dioctadecyl-3,3,3',3'-tetramethylindotricarbocyanine iodide),



the TMBM chimeric vesicles were incorporated into the hydrogel matrix to generate the HG-TMBMR formulation. The labeled HG-TMBMR hydrogel (100  $\mu\text{L}$ ) was subcutaneously injected into BALB/c mice. At designated intervals, fluorescence-based optical imaging was conducted on live subjects.

## 2.8 *In vitro* biocompatibility evaluation

To determine the biocompatibility of the HG-TMBMR preparation with non-cancerous cells, its potential cytotoxic effects on L929 murine fibroblasts were assessed *via* the CCK-8 colorimetric assay. Cells cultured under optimal conditions were released from the substrate using trypsin; the enzymatic reaction was subsequently quenched with complete DMEM, and the suspension was pelleted by centrifugation at 1000 rpm for 5 minutes. The pellet was gently dispersed, and a fresh medium was added and mixed to obtain the L929 cell suspension. The cell concentration was determined and adjusted to  $4 \times 10^4$  cells per mL. L929 cells were planted into 96-well culture plates and cultured overnight. Next, the HG-TMBMR hydrogel at various concentration gradients (the non-toxic concentration of Rg3 was verified with the identical protocol) was introduced into each well, and the cells were cultured for an additional 24 h. The supernatant was removed, and each well received 100  $\mu\text{L}$  of fresh culture medium supplemented with 10  $\mu\text{L}$  of the CCK-8 reagent. Following a 4-hour incubation period, optical density was recorded at 450 nm. Relative cell viability was determined according to the following formula:

$$\text{Cell viability ratio} = (A_{\text{sample}} - A_{\text{blank}}) / (A_{\text{positive}} - A_{\text{blank}}) \times 100\%$$

In this formula,  $A_{\text{sample}}$ ,  $A_{\text{positive}}$ , and  $A_{\text{blank}}$  denote the absorbance values measured at 450 nm for the experimental, positive control, and blank control groups, respectively.

## 2.9 Activation and maturation of bone marrow-derived DCs *in vitro*

DCs were differentiated from bone marrow progenitors obtained from BALB/c mice aged 6 to 8 weeks. Hind limb long bones (tibia and femur) were excised, and the marrow spaces were repeatedly perfused with RPMI 1640 to collect hematopoietic precursors. Following erythrocyte lysis, the cell suspension was filtered through a 70  $\mu\text{m}$  nylon strainer and subsequently cultured for 7 days in RPMI 1640 medium containing 20  $\text{ng mL}^{-1}$  GM-CSF and 10  $\text{ng mL}^{-1}$  IL-4. The resultant BMDCs were then incubated for 24 hours with various formulations: PBS (negative control), HG-TM, HG-BM, HG-TMBM, HG-Rg3, or the combinatorial HG-TMBMR. Subsequently, the BMDCs were harvested and labeled with fluorescein isothiocyanate (FITC) anti-mouse CD11c, allophycocyanin (APC) anti-mouse CD80, and phycoerythrin (PE) anti-mouse CD86 for flow cytometry (FCM) assessment. Upon termination of co-incubation, supernatants were harvested and cytokine levels were quantified using an enzyme-linked immunosorbent assay (ELISA).

## 2.10 *In vitro* recruitment ability of BMDCs

BMDCs were obtained as described above. A Transwell system was employed to evaluate the migratory capacity of BMDCs. In brief, DCs were placed in the apical compartment of the insert, while PBS, HG-TM, HG-BM, HG-TMBM, HG-Rg3, and HG-TMBMR were placed in the lower chamber. The concentration of the hybrid biofilms was standardized at 100  $\mu\text{g mL}^{-1}$  (based on the protein content). The recruitment of BMDCs across the polycarbonate membrane was assessed based on the recruitment capacity of the hybrid biofilm components. After 24 h, the immigrated cells were fixed, stained with crystal violet ammonium oxalate, and counted in five non-overlapping fields using an inverted microscope.

## 2.11 *In vitro* T cell proliferation assay

BMDCs were co-incubated with PBS, HG-TM, HG-BM, HG-TMBM, HG-Rg3, and HG-TMBMR for 24 h.  $\text{CD8}^+$  T lymphocytes were harvested from the spleens of BALB/c mice *via* immunomagnetic bead separation. Vaccine-activated BMDCs were co-incubated with carboxyfluorescein succinimidyl ester (CFSE)-labeled  $\text{CD8}^+$  T cells for 48 h at a DC-to-T cell ratio of 1:10. Cells were then harvested and analyzed by flow cytometry (FCM).

## 2.12 *In vivo* splenocyte killing assay

BALB/c mice aged six to eight weeks were assigned into six groups, and each group was administered 100  $\mu\text{L}$  of normal saline (NS), HG-TM, HG-BM, HG-TMBM, HG-Rg3, or HG-TMBMR *via* subcutaneous injection at the tail base, respectively. Seven days later, splenocytes were isolated by harvesting the spleens from euthanized mice and processing them into single-cell suspensions. CT26 cells were plated in 96-well culture plates at a density of 5000 cells per well and allowed to adhere. Splenocyte suspensions were then overlaid at 100 000 cells per well and maintained for 24 h. At the end of co-culture, the medium was removed and replaced with 100  $\mu\text{L}$  of fresh medium containing 10  $\mu\text{L}$  of CCK-8 solution. Following a further 4 h incubation, absorbance was measured at approximately 450 nm. Viability percentages were computed by comparing sample absorbance to that of the NS control group, employing the equation below:

$$\text{Cell viability ratio} = (A_{\text{sample}} - A_{\text{blank}}) / (A_{\text{positive}} - A_{\text{blank}}) \times 100\%$$

## 2.13 *In vivo* tumor prevention assay

BALB/c mice aged six to eight weeks were assigned into six groups, and each group was given a subcutaneous injection of 100  $\mu\text{L}$  of normal saline (NS), HG-TM, HG-BM, HG-TMBM, HG-Rg3, or HG-TMBMR at the tail base once per week. Twenty-one days later, the mice were subcutaneously implanted with  $1 \times 10^6$  CT26 tumor cells. The tumor volume was then monitored continuously thereafter. On the last day of the observation period, tumors were surgically removed from



euthanized mice and subsequently weighed to assess tumour burden.

#### 2.14 *In vivo* tumor treatment assay

BALB/c mice aged six to eight weeks were subcutaneously implanted with  $1 \times 10^6$  CT26 tumor cells. Seven days after tumor inoculation, each group was given a subcutaneous injection of 100  $\mu$ L of normal saline (NS), HG-TM, HG-BM, HG-TMBM, HG-Rg3, or HG-TMBMR. Tumor volume was monitored on an ongoing basis throughout the experiment. On the last day of the observation period, tumors were surgically removed from euthanized mice and subsequently weighed to assess tumour burden.

#### 2.15 *In vivo* immunoassays

At the conclusion of the prevention and therapy assays, mouse spleens and tumors were dissected for immunological assessment. Single-cell suspensions were derived from splenic tissue following erythrocyte lysis. To characterize T lymphocyte subsets, single-cell suspensions were stained with APC anti-mouse CD45, FITC anti-mouse CD4, and APC/cyanine7 anti-mouse CD8a, after which samples were analyzed *via* flow cytometry. For the determination of serum cytokine concentrations, serum was isolated by centrifuging blood samples from the tumor prevention experiment at 1000g for 15 minutes under refrigeration (4 °C); the recovered supernatant was subsequently subjected to ELISA quantification. For tumor tissues from mice in the tumor prevention assay, paraffin sections were prepared following fixation and analyzed by immunohistochemical staining and immunofluorescence staining. For tumor tissues from mice in the tumor treatment assay, paraffin sections were prepared following fixation and analyzed using a terminal deoxynucleotidyl transferase-mediated deoxyuridine triphosphate nick-end labeling (TUNEL) apoptosis detection kit.

#### 2.16 *In vivo* biocompatibility evaluation

BALB/c mice aged six to eight weeks were assigned into six groups, with each group receiving a subcutaneous injection of 100  $\mu$ L of normal saline (NS), HG-TM, HG-BM, HG-TMBM, HG-Rg3, or HG-TMBMR at the tail base, respectively. The body weight of each mouse was tracked longitudinally. At 21 days following the initial treatment, the animals were euthanized, and their cardiac, splenic, hepatic, pulmonary, and renal tissues were collected for histopathological assessment using H&E staining.

#### 2.17 Statistical analysis

The results are presented as the mean accompanied by the standard deviation (SD). Comparisons between two groups were conducted using Student's *t*-test, while comparisons involving multiple groups were analyzed *via* one-way analysis of variance (ANOVA), followed by Tukey's multiple comparisons test. Statistical significance is indicated as follows: \**p* < 0.05, \*\**p* < 0.01, \*\*\**p* < 0.001, and \*\*\*\**p* < 0.0001.

## 3. Results and discussion

### 3.1 Preparation and characterization of the HG-TMBMR hydrogel

Tumor cell membranes (TMs) and bacterial membranes (BMs) were obtained from the CT26 cell line and cultures of *L. reuteri*, respectively. The mixture of TMs and BMs was subjected to water bath sonication and then co-extruded *via* a polycarbonate membrane with a 400 nm pore diameter to realize biofilm fusion and acquire a hybrid biofilm (TMBM) with a suitable size. The resulting TMBM was further modified with methacrylated hyaluronic acid-gelatin methacrylate (HAMA-GelMA). Confocal microscopy verified the successful fusion of the biofilms, as the red fluorescence emitted by the TM labeled with DiD and the green fluorescence from the BM labeled with DiO showed colocalization (Fig. 2A). Likewise, protein analysis *via* SDS-PAGE revealed that the hybrid biofilm (TMBM) preserved all membrane proteins from both TM and BM, suggesting the effective extraction and hybridization of the two biofilms (Fig. 2B). Furthermore, the porous internal structure of the HG-TMBMR hydrogel before and after drug loading was characterized by SEM (Fig. 2C). Upon irradiation with 405 nm blue light, HG-TMBMR undergoes a sol-to-gel phase transition (Fig. 2D). Under photoinitiation, the methacrylate groups on HAMA and GelMA molecules undergo photopolymerization and covalent crosslinking, rapidly forming stable carbon-carbon (C-C) covalent bonds. These covalent bonds form a dense and stable three-dimensional polymer network, converting the liquid precursor into a solid-like hydrogel. *In vitro*, the HG-TMBMR hydrogel solution contained in the syringe could be easily injected, initially confirming the injectability of this hydrogel-based tumor vaccine (Fig. 2E). Additionally, we further assessed the *in vitro* release profile of the hydrogel, whose biofilm-releasing capability was reflected by the quantity of the liberated protein. Based on the release curve, 89.4% of the protein was continuously released from the HG-TMBMR hydrogel within 4 days (Fig. 2F), demonstrating that the hydrogel system exhibited controlled-release capability. As shown in Fig. 2G, the HG-TMBMR hydrogel was capable of persisting *in vivo* for a few days and degrading gradually within 40 days after subcutaneous injection.

### 3.2 *In vitro* immune effects of the HG-TMBMR hydrogel

The cytocompatibility of the HG-TMBMR hydrogel was determined by assessing its toxicity to normal cells. L929 fibroblasts were co-incubated with the HG-TMBMR hydrogel for 24 h, and the cells maintained excellent viability at various HG-TMBMR hydrogel concentrations, indicating superior cytocompatibility (Fig. 3A). To assess the immune-stimulating potential of the HG-TMBMR hydrogel, Transwell migration experiments and FCM were employed to evaluate the *in vitro* behavior of BMDCs, recruitment ability and maturation level, respectively. Quantification of migrated BMDC populations revealed that the HG-TMBMR hydrogel markedly promoted the migratory ability of DCs toward the hydrogel site (Fig. 3B and C). CD80 and CD86 are classic marker proteins expressed on mature



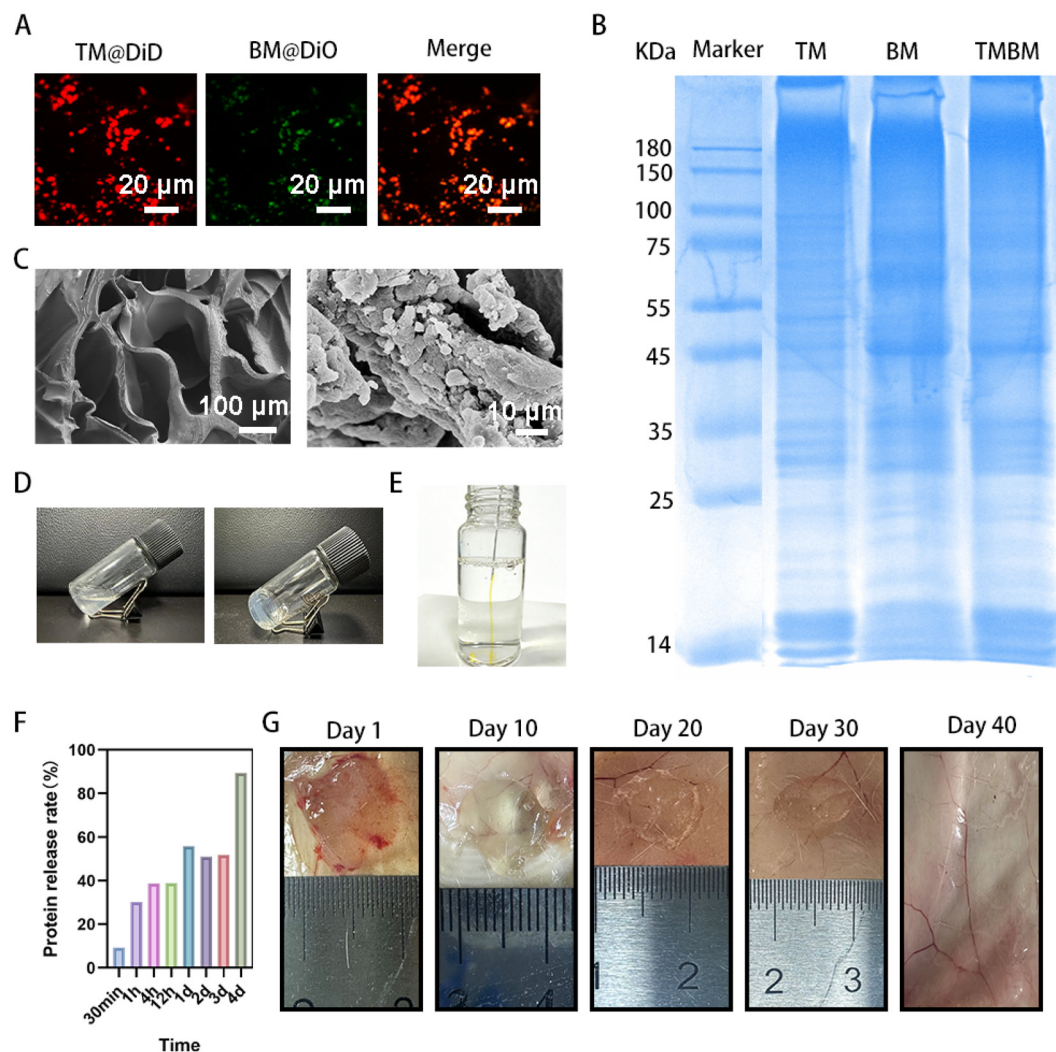


**Fig. 2** (A) Confocal microscopy image of the hybrid biofilm (TMBM). (B) SDS-PAGE protein analysis of TMBM. (C) SEM images of hydrogels before and after drug loading. (D) Photograph depicting the sol-to-gel transition following blue light irradiation. (E) Injection of the HG-TMBMR hydrogel (containing a small amount of phenol red for enhanced visualization) in phosphate-buffered saline (PBS) solution. (F) Release profile of biofilm proteins from the HG-TMBMR hydrogel. (G) Photographs showing the *in vivo* degradation profile of the HG-TMBMR hydrogel at different time points.

DCs, which deliver co-stimulatory signals necessary for naive T cell activation. Following co-incubation of BMDCs with the HG-TMBMR hydrogel, the co-expression levels of CD80 and CD86 were markedly elevated. The proportion of mature DCs reached 47.2%, a substantial increase relative to the 11.1% detected in the phosphate-buffered saline (PBS) control group, as presented in Fig. 3D and E. These findings show that the HG-TMBMR hydrogel functions as an antigen depot, substantially improving DC recruitment and maturation, thereby achieving robust and sustained T cell activation.

Concentrations of pro-inflammatory cytokines released by DCs after stimulation act as key markers to evaluate the immune efficacy of vaccines. Therefore, we further investigated the secretion of relevant pro-inflammatory cytokines by DCs following hydrogel treatment. Relative to the remaining experimental groups, the HG-TMBMR cohort displayed the peak concentrations of interleukin-6 (IL-6), interleukin-12p40

(IL-12p40), and tumor necrosis factor- $\alpha$  (TNF- $\alpha$ ) within the cell culture supernatants (Fig. 4A–C), indicating that the HG-TMBMR hydrogel exhibits potent capacity to induce DCs to release pro-inflammatory cytokines. Given the strong capacity of the HG-TMBMR hydrogel to induce DC activation, we further assessed its capacity to promote T cell proliferation. BMDCs pre-stimulated with the HG-TMBMR hydrogel were co-incubated with T cells for 48 h. The co-incubation was designed to evaluate the promoting effect of BMDCs matured by the hydrogel vaccine on the activation and proliferation of T cells, and to verify the cascade immune effect of the hydrogel vaccine through DC activation followed by the functional activation of T cells. As illustrated in Fig. 4D and E, HG-TMBMR hydrogel-stimulated BMDCs effectively promoted T cell proliferation. Collectively, the current results show that the HG-TMBMR hydrogel is capable of efficiently triggering DC stimulation and T cell activation *in vitro*, thereby eliciting



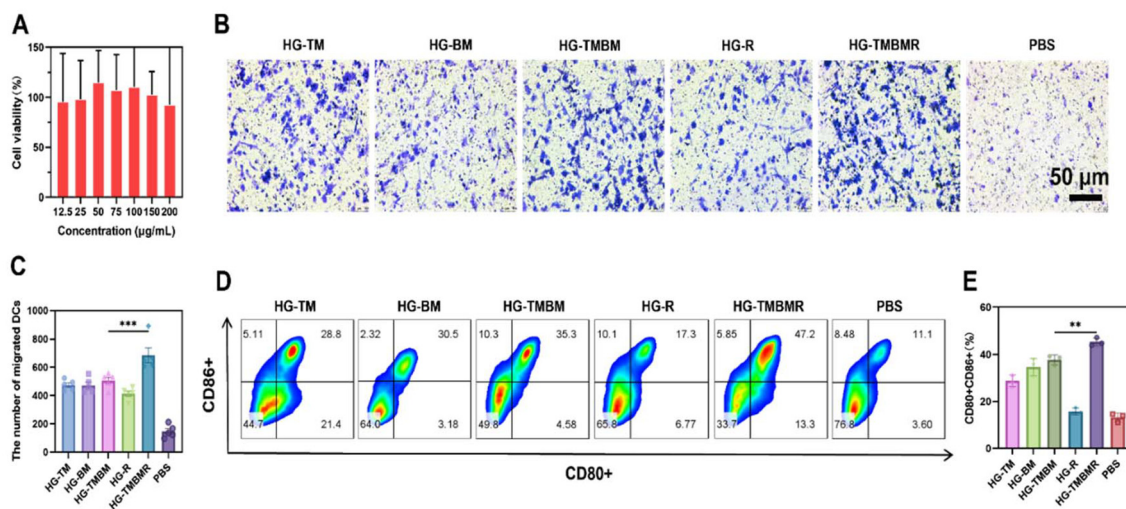


**Fig. 3** (A) The viability of L929 fibroblasts following exposure to different concentrations of the HG-TMBMR hydrogel ( $n = 6$ ). This concentration corresponds to the concentration of the biofilm membrane protein within the hydrogel, with a mass ratio of Rg3 to the biofilm membrane protein of 1:20. (B) Representative microscopy images. (C) Quantitative data related to DC migration were obtained via Transwell assays; the quantity of migrated cells was calculated by counting across five random visual fields ( $n = 3$ ). (D and E) FCM analysis illustrating the proportion of mature DCs after various treatment conditions. All experimental data are shown as the mean  $\pm$  standard deviation (SD). Levels of statistical significance are denoted as  $*p < 0.05$ ,  $**p < 0.01$ ,  $***p < 0.001$ , and  $****p < 0.0001$ .

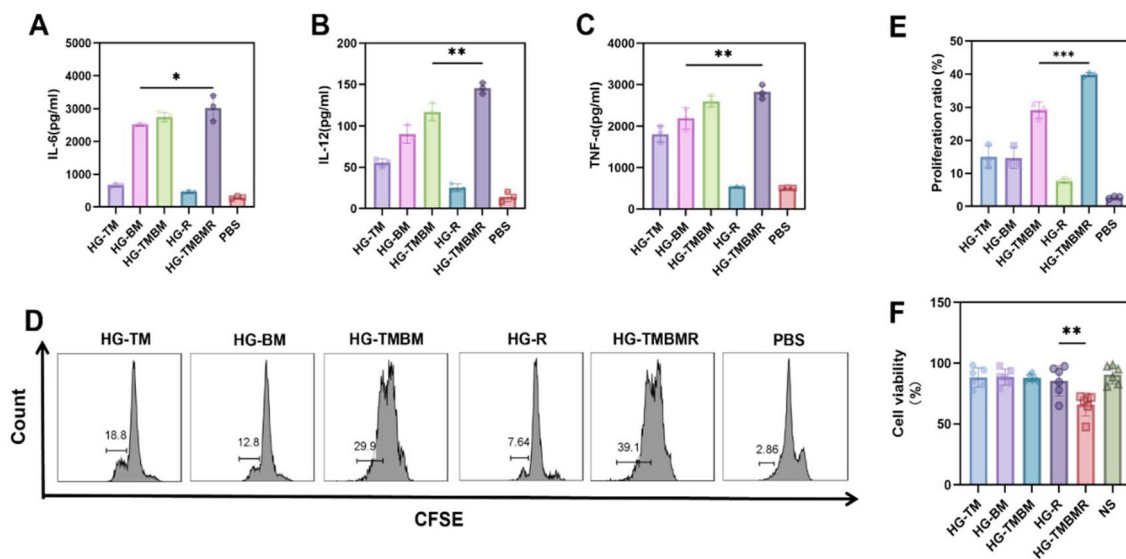


**Fig. 4** Release of (A) interleukin-6 (IL-6), (B) interleukin-12p40 (IL-12p40), and (C) tumor necrosis factor- $\alpha$  (TNF- $\alpha$ ) from BMDCs after various treatment regimens, measured using ELISA ( $n = 3$ ). (D and E) Quantitative data regarding T cell proliferation under different treatment conditions ( $n = 3$ ). (F) Viability of CT26 cells following co-incubation with splenocytes isolated from the treated mice ( $n = 6$ ). All experimental data are expressed as mean  $\pm$  standard deviation (SD). Statistical significance is denoted as  $*p < 0.05$ ,  $**p < 0.01$ ,  $***p < 0.001$ , and  $****p < 0.0001$ .

potent immunostimulatory functions. In addition, splenocytes obtained from mice that had been administered various formulations were co-cultured with CT26 tumor cells for the evaluation of their tumor cytotoxicity. As depicted in Fig. 4F, splenocytes from mice vaccinated with HG-TM alone exerted limited cytotoxicity against CT26 tumor cells, suggesting that immunization with antigen alone is insufficient to induce effective T cell activation. In contrast, the cellular viability

measured in the HG-TMBMR group was 66.1%, a value that was notably lower in comparison with every other test group. This enhanced tumor-killing capacity is attributed to the synergistic cooperation among the antigen, adjuvant, and immunomodulatory component (Rg3) within the HG-TMBMR hydrogel. Collectively, these results indicate that the HG-TMBMR tumor vaccine is capable of triggering strong T cell activation targeting tumor cells *via* the synergistic actions



of the antigen, adjuvant, and Rg3, thus inhibiting the degradation of antigens.

### 3.3 Assessment of *in vivo* tumor development prevention

Since antigens are integrated within the HG-TMBMR hydrogel framework, the hydrogel-based vaccine is anticipated to display extended *in vivo* persistence, thus preventing the rapid elimination of antigens by the immune system. To further explore the *in vivo* retention capacity, the hybrid biofilm (TMBM) was marked with the near-infrared fluorescent dye DiR, thus endowing the HG-TMBMR hydrogel vaccine with fluorescence characteristics. Mice were randomly assigned to two groups and administered with dye-marked preparations, followed by *in vivo* fluorescence imaging analysis at various time intervals. On day 12, the fluorescence signal intensity in the Rg3 + hybrid biofilm (TMBM) mixture group was significantly weakened, whereas that in the HG-TMBMR hydrogel group remained at a relatively high level (Fig. 5A and B). The weakened fluorescence was mainly attributed to the poor stability and rapid clearance of the free mixture *in vivo*, which lacked the sustained-release and protective effects of the hydrogel. In contrast, the hydrogel system could retain the biofilm and prolong its retention time, resulting in a stronger fluorescence signal. The capacity of the HG-TMBMR hydrogel vaccine to prevent tumor devel-

opment was further assessed in mice. Male BALB/c mice were administered different vaccine formulations. On day 21 post-immunization, the mice were subjected to a CT26 tumor cell challenge (defined as day 0), with continuous monitoring of tumor volumes conducted over the following three weeks. As shown in Fig. 5C and D, tumors generally developed in all groups by day 7. Notably, tumor volumes in the normal saline (NS) group and HG-Rg3 group increased rapidly during the subsequent 14 days. In contrast, tumor growth was most delayed in mice immunized with the HG-TMBMR hydrogel, indicating the favorable prophylactic effect of the vaccine on delaying tumor progression. Compared with the other groups, mice treated with the HG-TMBMR hydrogel also displayed the smallest tumor burden (Fig. 5E) and the lowest tumor weight (Fig. 5F). Additionally, the biological safety of the HG-TMBMR hydrogel tumor vaccine was systematically evaluated. No notable reduction in body weight was detected over the 21-day period post-immunization (Fig. 5G). In addition, H&E staining of the major organs in mice showed that the HG-TMBMR treatment did not induce pathological lesions in any organ (Fig. 5H). These findings verify that the HG-TMBMR hydrogel, serving as a prophylactic vaccine, can effectively delay tumor progression after a single immunization dose while ensuring favorable biological safety.

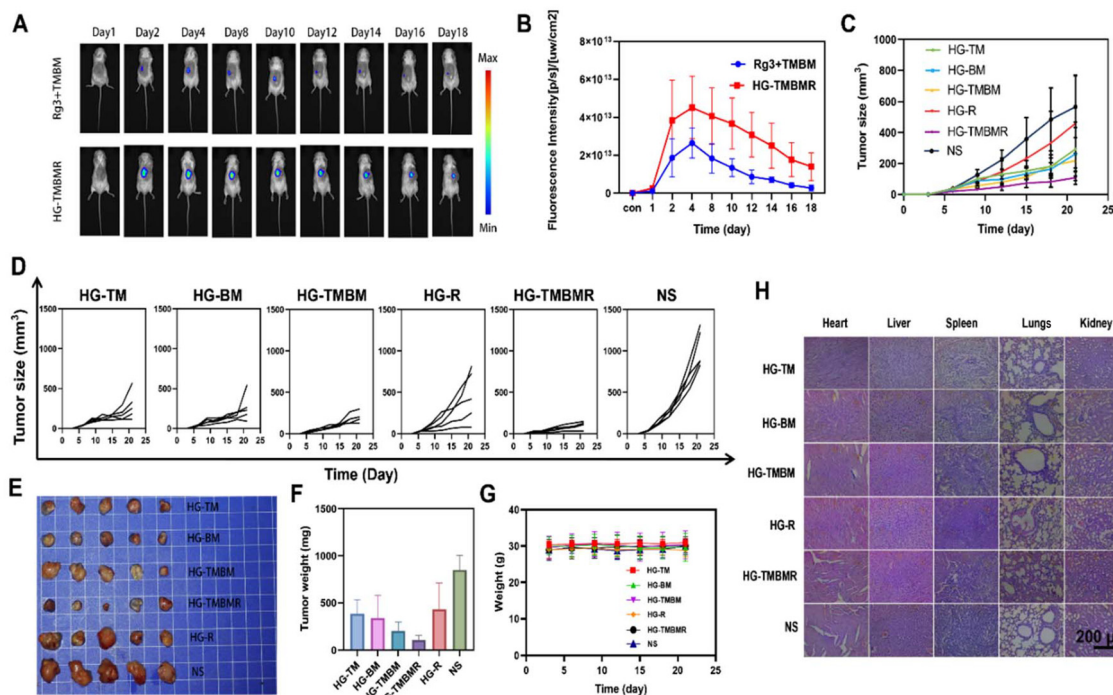


**Fig. 5** (A and B) *In vivo* retention profile of the Rg3 + hybrid biofilm (TMBM) mixture and HG-TMBMR hydrogel characterized by IVIS. (C) Mean tumor growth profiles of mice treated with distinct formulations ( $n = 5$ ). (D) Temporal changes in individual tumor growth for mice administered with various preparations ( $n = 5$ ). (E) Macroscopic tumor morphology and (F) tumor weight in mice following different therapeutic interventions ( $n = 5$ ). (G) Body weight of mice during the administration of diverse treatment regimens ( $n = 5$ ). (H) Representative H&E staining images of the major organs harvested from mice subjected to different treatments. All data are expressed as mean  $\pm$  standard deviation (SD). Statistical significance is defined as \* $p < 0.05$ , \*\* $p < 0.01$ , \*\*\* $p < 0.001$ , and \*\*\*\* $p < 0.0001$ .



To elucidate the immune mechanism responsible for the tumor-inhibitory activity of the hydrogel, immunized mice were humanely sacrificed on the 21st day for the collection and isolation of tumor tissues, spleen specimens, and serum samples. Tumor-infiltrating CTLs ( $CD3^+CD8^+$ ) and helper T lymphocytes ( $CD3^+CD4^+$ ) were quantified using FCM analysis. To explore the immune mechanism behind the tumor-preventive action of the hydrogel, vaccinated mice were sacrificed on day 21 to harvest tumors, spleens, and serum samples. Tumor-infiltrating CTLs ( $CD3^+CD8^+$ ) and helper T cells ( $CD3^+CD4^+$ ) were quantified by FCM (Fig. 6A–C). Meanwhile, the HG-TMBMR hydrogel vaccine significantly increased the serum levels of IFN- $\gamma$  and TNF- $\alpha$  (Fig. 6D and E). Immunofluorescence and immunohistochemical analyses of tumor-infiltrating CTLs revealed findings consistent with those observed in the spleen (Fig. 6F and G). Collectively, these results show that the HG-TMBMR hydrogel substantially increases the proportion of CTLs in both tumor tissues and spleens. Given the pivotal role of CTLs in tumor cell elimination, the delayed tumor pro-

gression observed in the HG-TMBMR hydrogel group is attributed to the hydrogel-mediated enhancement of CTL proportions and function.

### 3.4 Inhibition of tumor progression *in vivo*

In addition to the preventive capacity of the tumor vaccine, the anti-tumor activity of the HG-TMBMR hydrogel was further explored. Male BALB/c mice were randomly divided into six groups and inoculated with CT26 cells for the establishment of a mouse colon tumor model. On day 7 post-implantation, the mice were administered with HG-TM, HG-BM, HG-TMBM, HG-Rg3 and HG-TMBMR hydrogels, and normal saline (NS), respectively. Tumor growth was monitored continuously over a two-week period. As shown in Fig. 7A and B, treatment with the HG-TMBMR hydrogel significantly delayed tumor growth, demonstrating that the hydrogel vaccine could effectively suppress tumor progression. Compared with the other groups, mice treated with the HG-TMBMR hydrogel displayed a smaller tumor burden (Fig. 7C) and the lowest tumor weight (Fig. 7D). According to the survival profiles of mice across

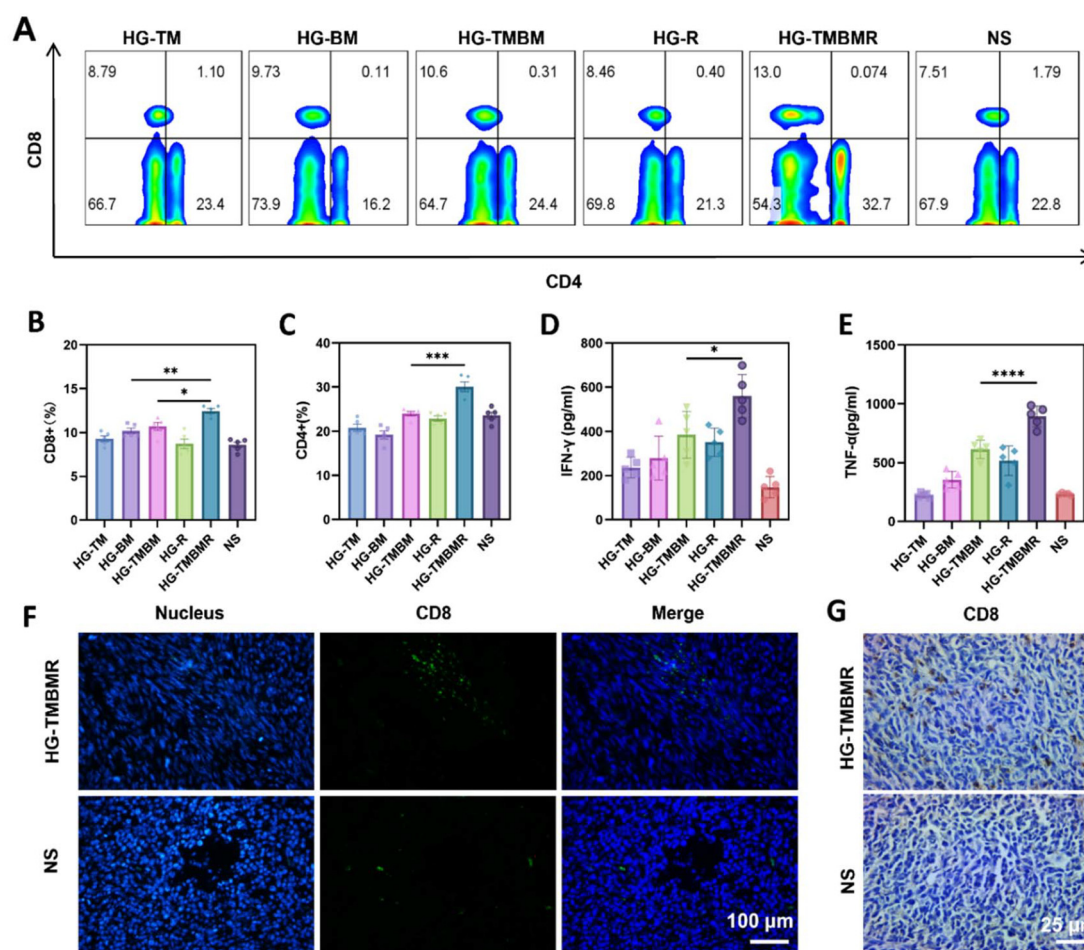


**Fig. 6** (A–C) Flow cytometric analysis showing the percentages of CTLs and helper T cells in the spleen. (D) IFN- $\gamma$  and (E) TNF- $\alpha$  levels in serum ( $n = 3$ ). (F) Immunofluorescence images of CTLs in tumors. (G) Immunohistochemical staining images of CTLs in tumors. Experimental data are expressed as the mean  $\pm$  standard deviation (SD). Statistical significance is labeled as \* $p < 0.05$ , \*\* $p < 0.01$ , \*\*\* $p < 0.001$ , and \*\*\*\* $p < 0.0001$ .



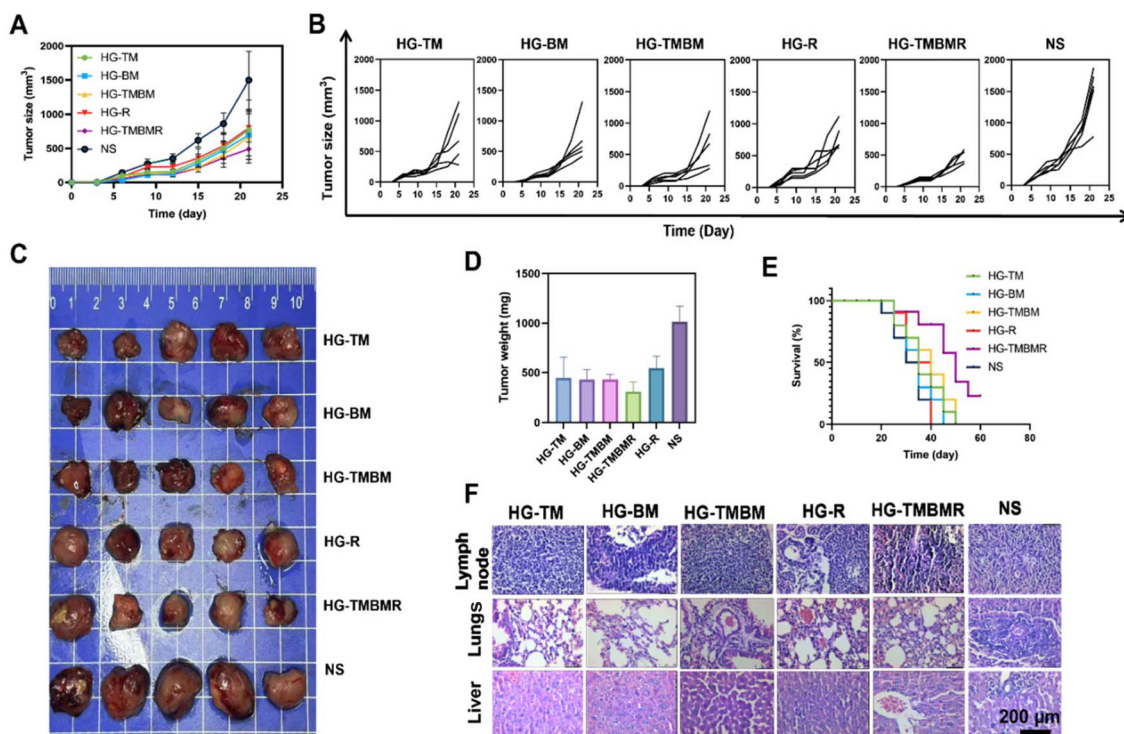


**Fig. 7** (A) Average tumor growth profiles of mice treated with distinct formulations ( $n = 5$ ). (B) Tumor growth kinetics of individual mice receiving different formulations ( $n = 5$ ). (C) Tumor morphology and (D) tumor weight of mice after different treatment regimens ( $n = 5$ ). (E) Survival curves of mice given different formulations ( $n = 10$ ). (F) H&E staining images of the major organs of mice subjected to various treatments. Experimental data are expressed as the mean  $\pm$  standard deviation (SD). Statistical significance is labeled as  $*p < 0.05$ ,  $**p < 0.01$ ,  $***p < 0.001$ , and  $****p < 0.0001$ .

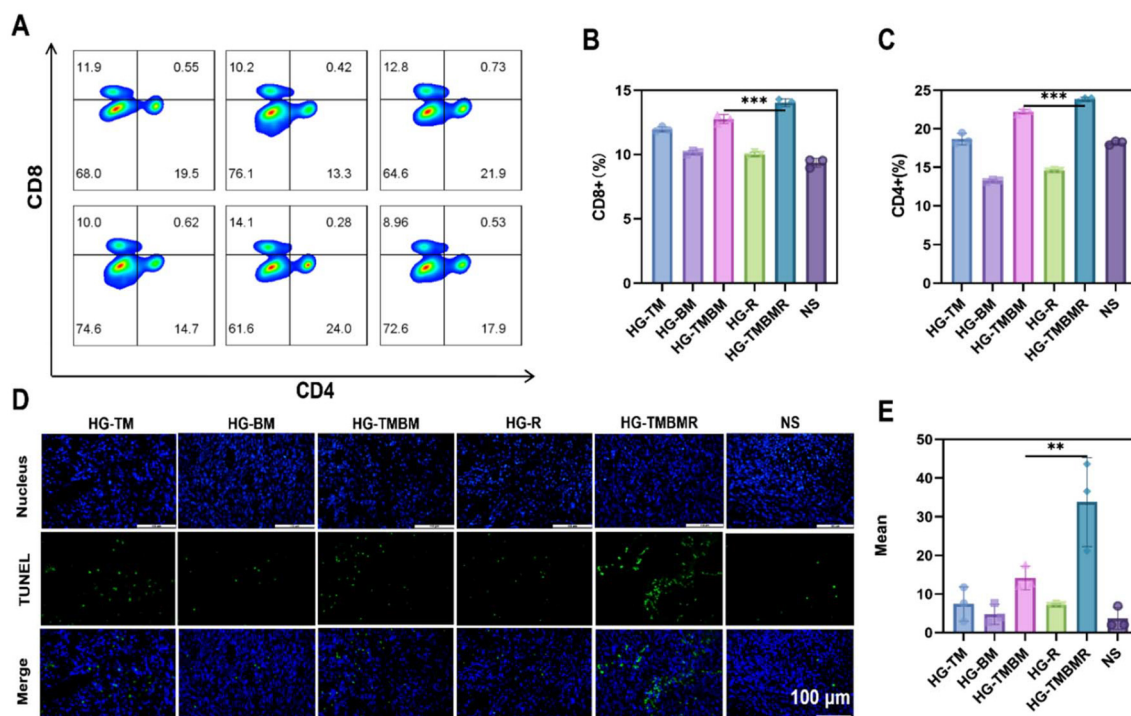


**Fig. 8** (A–C) FCM analysis showing the percentages of CTLs and helper T cells in the spleen. (D and E) Fluorescence images of terminal deoxynucleotidyl transferase-mediated dUTP nick-end labeling (TUNEL) staining, along with a quantitative assessment of tumor cell apoptosis. All experimental data are expressed as the mean  $\pm$  standard deviation (SD). Statistical significance is indicated as  $*p < 0.05$ ,  $**p < 0.01$ ,  $***p < 0.001$ , and  $****p < 0.0001$ .



various groups (Fig. 7E), treatment with the HG-TMBMR hydrogel markedly extended the survival period of tumor-bearing mice. At the conclusion of the therapeutic experiment, the mice were humanely sacrificed, and their major organs were subjected to H&E staining. The findings revealed that, in comparison with the NS group, administration of the HG-TMBMR hydrogel suppressed local tumor metastasis (Fig. 7F).

CTLs ( $CD3^+CD8^+$ ) and helper T cells ( $CD3^+CD4^+$ ) that infiltrated the tumor were identified *via* FCM. As illustrated in Fig. 8A–C, mice administered with the HG-TMBMR hydrogel displayed strengthened anti-tumor immune responses, since the proportions of both CTLs and helper T cells within the tumor tissue were the highest across all treatment groups. The fluorescence images from the apoptosis assay in the HG-TMBMR hydrogel group (Fig. 8D and E) further confirmed that the tumor vaccine suppressed tumor progression by promoting tumor cell apoptosis. Taken together, these findings indicate that the HG-TMBMR hydrogel, acting as a prophylactic vaccine, is capable of not only effectively inhibiting tumor formation but also functioning as a therapeutic vaccine to delay the progression of tumors.

## 4. Conclusion

In summary, the present study constructed an injectable hydrogel integrated with biofilm, which serves as a one-dose, highly effective prophylactic vaccine targeting colon cancer, designed to achieve potent and long-lasting immune activation. The hybrid biofilm (TMBM), modified with HAMA-GelMA, was fabricated into a hydrogel formulation (HG-TMBM hydrogel), and Rg3 was encapsulated within the micropores of the hydrogel to establish a stable sustained-release system for antigens and bioactive components. Upon subcutaneous injection, the system rapidly undergoes a sol-to-gel transition, and the gradual degradation of the matrix enables a slow and sustained release of the hybrid biofilm (TMBM) and Rg3. The hybrid biofilm (TMBM) can actively target DCs and efficiently induce their maturation, while Rg3 modulates the immune microenvironment and enhances antigen presentation efficiency. The synergistic action of these two components promotes the activation, proliferation, and functional stability of CTLs, enhances specific antitumor immune responses and successfully surmounts the key limitations of conventional prophylactic vaccines, including insufficient immune activation intensity and the requirement for multiple administrations. The enhanced and long-lasting T lymphocyte-mediated immune response induced by this hydrogel vaccine provides substantial prophylactic efficacy against colon cancer. The long-lasting tumor prevention platform constructed in the present research offers a novel technological approach for the innovative advancement of single-dose prophylactic cancer vaccines and is anticipated to facilitate the clinical transformation of prophylactic cancer vaccines.

## Author contributions

Chaoying Wang contributed to conceptualization, formal analysis, data curation and core investigation. Tao Wang (co-equal contributor) led conceptualization, supervised the research, participated in funding acquisition and edited the manuscript. Wenxin Zhou (another co-equal contributor) spearheaded conceptualization and methodology design. Other authors provided experimental and investigative support. The corresponding authors Wei Wu and Quan Zhang led overall project design, supervision, funding acquisition and manuscript revision.

## Conflicts of interest

There are no conflicts to declare.

## Data availability

All datasets generated and analyzed in this study are openly available.

## Acknowledgements

This work was supported by the Yangzhou University Medical Innovation and Transformation Special Fund (project number: AHYZUCXTD202104).

## References

- 1 L. Zhang, Y. Xiang, Y. Li and J. Zhang, Gut microbiome in multiple myeloma: Mechanisms of progression and clinical applications, *Front. Immunol.*, 2022, **13**, 1058272.
- 2 M. Zhang, Y. Wang, Z. Song, Y. Lu, H. Zhao, Y. Wang, *et al.*, Recent Progress of Bioinspired Cell Membrane in Cancer Immunotherapy, *Clin. Med. Insights: Oncol.*, 2024, **18**, 11795549241236896.
- 3 M. Kaczmarek, J. Poznańska, F. Fechner, N. Michalska, S. Paszkowska, A. Napierała, *et al.*, Cancer Vaccine Therapeutics: Limitations and Effectiveness-A Literature Review, *Cells*, 2023, **12**(17), 2159.
- 4 Y. Yang, X. Zhang, Y. Gao, Y. Dong, D. Wang, Y. Huang, *et al.*, Research Progress in Immunotherapy of NSCLC With EGFR-Sensitive Mutations, *Oncol. Res.*, 2022, **29**(1), 63–74.
- 5 P. Abdollahi, H. M. Norseth and F. Schjesvold, Advances and challenges in anti-cancer vaccines for multiple myeloma, *Front. Immunol.*, 2024, **15**, 1411352.
- 6 D. Ren, S. Xiong, Y. Ren, X. Yang, X. Zhao, J. Jin, *et al.*, Advances in therapeutic cancer vaccines: Harnessing immune adjuvants for enhanced efficacy and future perspectives, *Comput. Struct. Biotechnol. J.*, 2024, **23**, 1833–1843.



- 7 C. Y. Chiang, Y. J. Chen, C. C. Wu, S. J. Liu, C. H. Leng and H. W. Chen, Efficient Uptake of Recombinant Lipidated Survivin by Antigen-Presenting Cells Initiates Antigen Cross-Presentation and Antitumor Immunity, *Front. Immunol.*, 2018, **9**, 822.
- 8 M. Haug, G. Brede, M. Håkerud, A. G. Nedberg, O. A. Gederaas, T. H. Flo, *et al.*, Photochemical Internalization of Peptide Antigens Provides a Novel Strategy to Realize Therapeutic Cancer Vaccination, *Front. Immunol.*, 2018, **9**, 650.
- 9 X. Wang, L. Liu, Y. Chen, L. Jia, Y. Wang, W. Jing, *et al.*, MgZnFe-layered double hydroxides as a dual-function platform for enhancing subunit vaccine efficacy in tumor immunotherapy, *Int. J. Pharm.: X*, 2025, **10**, 100384.
- 10 H. Li, H. Wen, H. Zhang, J. Li, X. Cao, J. Zhang, *et al.*, Polymeric micelle-hydrogel composites design for biomedical applications, *Chin. Chem. Lett.*, 2025, **36**(5), 110072.
- 11 W. Chen, K. Shi, Y. Yu, P. Yang, Z. Bei, D. Mo, *et al.*, Drug delivery systems for colorectal cancer chemotherapy, *Chin. Chem. Lett.*, 2024, **35**(2), 109159.
- 12 Y. Gao, R. Zhou, Q. Wang, S. Qi, Y. Lv, S. Liu, *et al.*, Natural killer cell membrane doped supramolecular nanoplatform with immuno-modulatory functions for immuno-enhanced tumor phototherapy, *Chin. Chem. Lett.*, 2024, **35**(10), 109521.
- 13 M. Wang, D. Hu, Y. Yang, K. Shi, J. Li, Q. Liu, *et al.*, Enhanced Chemo-Immunotherapy Strategy Utilizing Injectable Thermosensitive Hydrogel for The Treatment of Diffuse Peritoneal Metastasis in Advanced Colorectal Cancer, *Adv. Sci.*, 2023, **10**(35), 2303819.
- 14 Y. Wang, X. Huang, Q. Wu and C. Gong, Biomimetic nanosystems based on cell membranes (BNCMs) for cancer immunotherapy, *MedComm: Biomater. Appl.*, 2024, **3**(4), e106.
- 15 J. Zhou, S. Zou, D. Dai, L. He, X. Mou, N. Zhao, *et al.*, Bacterial Outer Membrane Vesicles: From Physics to Clinical, *MedComm: Biomater. Appl.*, 2025, **4**(2), e70013.
- 16 D. Zhang, Q. Song, W. Wang, Q. Li, Z. Zhao, Y. Jiang, *et al.*, Unleashing a Dual-Warhead Nanomedicine to Precisely Sensitize Immunotherapy for Pancreatic Ductal Adenocarcinoma, *Adv. Funct. Mater.*, 2024, **34**(30), 2315447.
- 17 X. Gao, Q. Feng, J. Wang and X. Zhao, Bacterial outer membrane vesicle-based cancer nanovaccines, *Cancer Biol. Med.*, 2022, **19**(9), 1290–1300.
- 18 T. Neuper, T. Frauenlob, M. Sarajlic, G. Posselt, S. Wessler and J. Horejs-Hoeck, TLR2, TLR4 and TLR10 Shape the Cytokine and Chemokine Release of *H. pylori*-Infected Human DCs, *Int. J. Mol. Sci.*, 2020, **21**(11), 3897.
- 19 X. Zhao, R. Zhao and G. Nie, Nanocarriers based on bacterial membrane materials for cancer vaccine delivery, *Nat. Protoc.*, 2022, **17**(10), 2240–2274.
- 20 A. Kang, T. Xie, D. Zhu, J. Shan, L. Di and X. Zheng, Suppressive Effect of Ginsenoside Rg3 against Lipopolysaccharide-Induced Depression-Like Behavior and Neuroinflammation in Mice, *J. Agric. Food Chem.*, 2017, **65**(32), 6861–6869.
- 21 S. L. Lu, Y. H. Wang, G. F. Liu, L. Wang, Y. Li, Z. Y. Guo, *et al.*, Graphene Oxide Nanoparticle-Loaded Ginsenoside Rg3 Improves Photodynamic Therapy in Inhibiting Malignant Progression and Stemness of Osteosarcoma, *Front. Mol. Biosci.*, 2021, **8**, 663089.
- 22 S. Adepu and S. Ramakrishna, Controlled Drug Delivery Systems: Current Status and Future Directions, *Molecules*, 2021, **26**(19), 5905.
- 23 T. Thambi, Y. Li and D. S. Lee, Injectable hydrogels for sustained release of therapeutic agents, *J. Controlled Release*, 2017, **267**, 57–66.
- 24 B. Liu, J. Wu, X. Sun, Q. Meng and J. Zhang, Sustained delivery of osteogenic growth peptide through injectable photoinitiated composite hydrogel for osteogenesis, *Front. Bioeng. Biotechnol.*, 2023, **11**, 1228250.
- 25 H. Zhang, Y. Zhang, H. Hu, W. Yang, X. Xia, L. Lei, *et al.*, In Situ Tumor Vaccine for Lymph Nodes Delivery and Cancer Therapy Based on Small Size Nanoadjuvant, *Small*, 2023, **19**(33), e2301041.

